AIAA 92-3546
Rayleigh Scattering Measurements of Shock Enhanced Mixing

John M. Budzinski, Edward E. Zukoski, and Frank E. Marble,

California Institute of Technology, Pasadena, CA

AIAA/SAE/ASME/ASEE
28th Joint Propulsion Conference and Exhibit
July 6-8, 1992 / Nashville, TN

RAYLEIGH SCATTERING MEASUREMENTS OF SHOCK ENHANCED MIXING

John M. Budzinski,* Edward E. Zukoski,** Frank E. Marble***

California Institute of Technology, Pasadena, California 91125

Abstract

This investigation was concerned with the mixing which occurs after the unsteady interaction of a shock wave with a laminar jet of helium. The jet of helium was injected normal to the direction of the propagation of the shock. The primary diagnostic, planar Rayleigh scattering, had sufficient spatial and temporal resolution to resolve the smallest diffusion scales present and allowed helium mole fractions to be measured in two-dimensional planes normal to the original jet flow direction. The amount of molecular mixing was evaluated with a mass distribution function at increasing times after the shock interaction. The total masses of helium contained in regions where the molar concentration of helium was at least 30% and 50% were also calculated. The shock Mach number was varied, and the effect of a reflected shock was studied. It was found that shock interactions can significantly increase the mixing between the air and helium. A rough collapse of the mixing data occurs when time is normalized by the jet radius divided by the change in velocity of the air behind the shock. An increase in the enhancement of mixing occurred after the interaction with the reflected shock.

Nomenclature

$()_0$	pertaining to the initial conditions, before the shock interaction
$()_1$	pertaining to the conditions before the shock interaction
$()_2$	pertaining to the conditions after the shock interaction
$()_{air}$	pertaining to pure air
$()_{cmf}$	pertaining to the center of mass fraction
$()_{He}$	pertaining to pure helium
$()_l$	pertaining to the light gas
$()_v$	pertaining to the vortex pair
α	molecular scattering cross section.
a	the speed of sound
A	area
χ	mole fraction
d	diameter of the jet cross section based on the region of 50% jet fluid
D	jet exit diameter
$\mathcal{D}$	diffusion coefficient
ε	strain rate
f	mass fraction
γ	specific heat ratio
Γ	circulation
h	height above the jet exit
m	mass distribution function
M	shock Mach number
M_{tot}	total mass of helium
ν	kinematic viscosity
n	number density of molecules
p	pressure
ρ	density
r_0	initial jet cross section radius based on the region of 50% jet fluid
t	time
τ	characteristic time scale
u	velocity of the air behind the shock
ω	vorticity
x	x coordinate (direction of shock propagation)
y	y coordinate

Introduction

Background

A vehicle using an air breathing engine while traveling at hypersonic speeds will require the air passing through the engine to remain supersonic relative to the airframe while mixing and combustion occur with the fuel. The time available for mixing between the air and hydrogen fuel is greatly reduced compared to a more conventional subsonic engine. For example, a typical vehicle traveling at Mach 15, may have the air in the combuster at Mach 5 with a velocity of 4000 m/s. Given the fact that the combustion chamber can only be a few meters long, the air will only be in the engine for 1-2 milliseconds.

Additional concern over the mixing is caused by the fact that the shear layers which form between the fuel and

---

* Graduate Student in Aeronautics, now Research Fellow in Mechanical Engineering.

** Professor of Mechanical Engineering and Jet Propulsion, Fellow AIAA.

*** Professor of Mechanical Engineering and Jet Propulsion, Emeritus, Fellow AIAA.

air will most likely be compressible, and compressible shear layers have growth rates much smaller than incompressible shear layers (Papamoschou and Roshko 1988). The mixing due to the shear of the flow will be less than that for more conventional subsonic engines. These realities facing the designers of supersonic combustion engines generate the need for mechanisms to augment the mixing process.

Such a mechanism, proposed by Marble, et al. (1987), uses weak shock waves inside the engine to enhance the mixing between the fuel and air. The concept is envisioned as a three-dimensional steady interaction between a jet of hydrogen and an oblique shock wave. The enhancement in mixing is driven by the baroclinic term in the vorticity equation:

$$\rho \frac{d}{dt}\left(\frac{\omega}{\rho}\right) = \frac{1}{\rho^2}\nabla\rho \times \nabla p \ .$$

The pressure gradient of the shock wave interacts with the density gradients between the air and hydrogen fuel to generate vorticity, which increases strain rates and enhances the rate of molecular scale mixing due to diffusion. This interaction is an example of the shock-induced Rayleigh-Taylor instability, or Richtmyer-Meshkov instability. Experimental and computational studies of injectors based on the shock-jet interaction were carried out by Waitz, et al. (1991, 1992), and computational studies including combustion were performed by Drummond, et al. (1991).

Analogies have been made between the three-dimensional steady shock-jet interaction and the two-dimensional unsteady interaction of a shock wave passing over a a cylindrical volume of lower density fluid (Marble et al. 1987, 1990, and Yang 1991). This analogy is shown in Figure 1; in a Lagrangian sense, the cross sections of the jet essentially undergo the same interaction in each case.

One of the earliest studies on the unsteady interaction of a shock with a cylindrical region of lower density fluid was performed by Rudinger and Somers (1960) in which the cylindrical volumes were created with jets of different density gases injected normal to the shock propagation direction. The purpose of the study was to illustrate that tracer bubbles of different density gases used for flow visualization or velocity measurements will not exactly move with the surrounding flow if they undergo accelerations.

Haas and Sturtevant (1987) studied the interaction of weak shocks with cylindrical volumes confined by microfilm membranes to model how finite-amplitude waves in random media generate turbulence. These experiments examined the wave patterns that developed and showed the deformation of the initial cylindrical volume. It was the results of the experiments of Haas and Sturtevant that motivated Marble et al (1987) to suggest that shock waves be used to enhance the mixing in supersonic combustion engines. Computations modeling the experiments of Haas and Sturtevant were performed by Picone and Boris (1987) and by Marble, et al (1987).

An experimental study of shock interactions with laminar jets of helium was performed by Jacobs (1992), who viewed the jet after the shock interaction with the planar laser induced fluorescence of a tracer dye, biacetyl (2,3-Butanedione), which was premixed with the helium. Finally, the most comprehensive computations of the unsteady interaction were performed by Yang (1991).

These investigations have developed a fundamental understanding of the general flow characteristics and have shown that the vorticity generated at the boundaries of the cylindrical volume during the shock interaction causes a stream of air to divide the initial circular cross section into two lobes. Each lobe is further divided into a tail region and a vortex core. The vortex cores from each lobe form a vortex pair that pulls ahead of the tail regions. The effect of the overall flow development is to generate straining motions which increase the area of the air-helium interface and enhance the mixing.

Yang (1991) used a similarity argument based on the vorticity equation to predict that the total circulation about each vortex should be:

$$\Gamma = 4 r_0 u \frac{\rho_1}{\rho_2}\left(\frac{1-\frac{\rho_t}{\rho_h}}{1+\frac{\rho_t}{\rho_h}}\right) .$$

Marble (1990) suggested that a characteristic scaling time for weak shock interactions where the lateral compression is negligible is $\tau = (r_0)^2/\Gamma$. Yang (1991) suggested for stronger shocks that $\tau = HW/\Gamma$ where H is a characteristic height which is represented by the initial radius r_0, and W is a characteristic width which includes the lateral compression due to the shock and is represented by $W = (\rho_1/\rho_2)r_0$ so that $\tau = (\rho_1/\rho_2)(r_0^2/\Gamma)$. Using the above expression for the circulation:

$$\tau \propto \frac{r_0}{u}\left(\frac{1+\frac{\rho_t}{\rho_h}}{1-\frac{\rho_t}{\rho_h}}\right) \propto \frac{r_0}{a_1}\left(\frac{M}{M^2-1}\right)\left(\frac{1+\frac{\rho_t}{\rho_h}}{1-\frac{\rho_t}{\rho_h}}\right)$$

For the purposes of this paper τ is defined to be equal to the expression on the right.

Another non-dimensional time which has been used by Marble (1990), and Yang (1991) is $a_1 t/r_0$, which is important because it easily allows the flow studied in an experiment to be compared to the real flow in an engine. For a real engine a typical value for the ambient speed of sound is about 800 m/sec and a typical jet radius about 1

cm. Since the fuel will only be in the engine for 1-2 ms, the mixing must by the time $a_1 t/r_0$ is in the range 80 to 160.

Although the overall flow development has been well characterized, the previous investigations have only been able to infer limited information on the degree of molecular scale mixing which occurs. In general, the results from computations regarding molecular mixing for these types of flows are not considered to be reliable. In addition, the previous experiments have not been able to measure molar helium concentrations with sufficient temporal and spatial resolution to represent molecular mixing. Experiments by Haas and Sturtevant (1987) were limited to shadowgraph photography. The experiments of Jacobs (1992) could not measure helium concentrations because of the differential diffusion between the helium and biacetyl. Concentration measurements by Waitz (1991) for the three-dimensional steady interaction were not spatially or temporally resolved.

Present Experiments

The goal of the present study was to measure the molecular scale mixing that occurs after the interaction of a shock with a laminar jet of helium. The experiments of the present study are illustrated in Figure 2 where a shock wave travels from left to right down a shock tube and interacts with a laminar jet of helium flowing out of the page. The shock accelerates the helium jet to the right, the cross section of the jet deforms, and the shock continues down the tube. A vortex pair forms from the helium jet. The shock reflects off the tube's end wall, travels back from right to left and interacts with the vortex pair. Experiments were performed that viewed a cross section of the jet with planar Rayleigh scattering, or imaged a side view of the jet with shadowgraph photography (the planar Rayleigh scattering was not done simultaneously with shadowgraph).

The Rayleigh scattering technique allowed a direct measure of the molar air concentration, χ_{air}, in a two-dimensional cross section and the helium concentration, χ_{He}, was found from $\chi_{He} = 1 - \chi_{air}$. The resolution of the measurements was sufficient to temporally and spatially resolve the smallest strained diffusion scales present in the laminar flow and allowed the amount of molecular mixing to be measured.

To understand the scaling of the mixing with increasing shock strength the shock-jet interaction was studied for three different shock Mach numbers: 1.07, 1.14, and 1.50. In addition, the effect of the reflected shock interaction was studied for Mach numbers 1.07, and 1.14. To keep the pressures in the test section after the reflected shock within the safe limits of the structure, the driven section of the shock tube was pumped down for the shock Mach number 1.50 experiments. In addition, the 1.14 Mach number interactions were studied with the pressure in the test section before the shock at 1 atmosphere, and at 0.55 atmospheres. Table 1 summarizes the conditions studied.

Table 1.

Mach #	Waves	p_1 (atm)
1.07	initial & reflected	1.0
1.14	initial	1.0
1.14	initial & reflected	0.55
1.50	initial	0.23

Since the scattering signal is proportional to the number density of molecules, the signal was strongest for the cases with the highest number density of molecules after the shock interaction, and the order of the listing in Table 1 coincides with the order of decreasing scattering signal strength.

For the cases with the jet initially at one atmosphere, the jet had a helium volumetric flow of 60 cm^3/sec. This resulted in an average velocity of 130 cm/sec at the exit and a Reynolds number of 75 based on the average velocity, the jet diameter, and the kinematic viscosity of helium. For the cases where the initial pressure was below atmospheric in the test sections, the jet Reynolds number was kept at 75 by keeping the helium mass flow rate the same.

For Mach numbers 1.07, and 1.50 the plane of the laser sheet intersected the helium jet 5.7 diameters above the jet exit. For the Mach 1.15, some experiments were performed with the laser sheet 4.9 diameters above the jet exit, and some with the laser sheet 5.7 diameters above the jet exit. At these distances air had diffused into the center of the jet. Table 2 summarizes, for the different cases studied, the height of the laser sheet plane above the jet exit, the center line molar helium concentration $\chi_{He}(r=0)$, and the radius of the jet cross section (based on the radius at which the concentration was 1/2 the center line concentration).

Table 2.

Case Mach#,p_1	h/D	$\chi_{He}(r=0)$	r_0 (cm)
1.07, 1 atm	5.7	0.89	0.46
1.14, 1 atm	4.9	0.92	0.45
1.14, 0.55 atm	4.9	0.94	0.55
1.14, 0.55 atm	5.7	0.92	0.55
1.50, 0.23 atm	5.7	0.92	0.62

Experimental Apparatus

The present study was performed in the GALCIT 17 inch shock tube (Liepmann et al. 1962); a side view of the driven section is shown in Figure 3. The transition from the circular 17 inch diameter cross section of the main tube to the 10.5 inch square cross section of the test sections was aided by a "cookie cutter" that prevented the waves caused by the change in cross sectional area from

interfering with the experiment. Two 2 ft long test sections could be attached in series to the cookie cutter; the first had a 6 inch diameter window on the bottom, while the second had two 6 inch diameter windows on its sides. A back end plate, also with a 6 inch diameter window, closed the tube. All of the windows were flush with the walls of the test sections or end plate.

The main shock tube and the test sections were each fitted with two model 112A21 PCB piezoelectric pressure transducers. The output of pressure transducers was recorded on an RC Electronics Model ISC-67 Computerscope board installed in an IBM model AT computer. The shock wave velocities were found by dividing the known distance between the transducers by the time for the shock to travel from one transducer to the next. The Mach number was calculated by dividing the velocity with the speed of sound for air at the measured temperature. The transducers were also used to trigger a Stanford Research System model DG535 digital delay/pulse generator which controlled the timing of the data acquisition systems.

Planar Rayleigh scattering was the primary diagnostic used in the investigation. To implement the scattering technique, cylindrical lenses were used to transform a 4J, 700 nsec long laser beam pulse at 480 nm, which was generated by a Candela SLL-1050M flashlamp pumped dye laser, into a thin sheet of light. The laser sheet, which was less than 1.5 mm thick, intersected a cross section of the deforming helium jet, and the light scattering off the molecules generated an image in the plane of the laser sheet that was captured by a Photometrics Star I cooled CCD camera. In the picture, the air was bright and the helium was dark. A calibration procedure was used to account for the variations in light intensity not related to the concentration variations. The CCD had an array of 576 by 384 square pixels each 20 microns on a side. The Star I system came with a camera controller with a 12 bit A/D converter which could read out and store one image at a time. The images were transferred from the camera controller to a Gateway 2000 386/33 AT compatible computer through an IEEE-488 GPIB board installed in the computer. Only one picture could be taken each time the shock tube was fired; a sequence was built by performing multiple experiments.

To complement the scattering technique, additional experiments were performed in which a standard spark shadowgraph system imaged a side view of the jet, using a Nanolamp spark light source, and either a 35 mm camera, or a General Electric TN2505 CID camera connected to a Poynting Products PC-170 frame grabber in an IBM/AT computer. The jet for a shadowgraph experiment was placed in one of the two locations in test section 2 shown in Figure 3. The position in the center of the window was used for pictures taken shortly after the shock interaction. The location upstream of the windows in the second test section was used for viewing the jet at longer times after the shock interaction.

The nozzle of the helium jet, which extended two inches into the test section through the bottom wall, was a brass tube with an I.D. of 0.305 inches (0.D. of 3/8"). The helium was supplied by a high pressure bottle, passed through a pressure regulator, monitored by a pressure gauge, and passed through a rotameter with a needle valve on its exit, before entering the test section. The helium in the test section was removed by a 9/16" diameter exit orifice, connected to a Welsh vacuum pump, and located above the helium jet, flush with the upper wall of test section 1.

After the shock wave interacted with the helium jet, it continued down the shock tube and reflected off the end plate. With both test sections in place the distorted helium jet would translate past the window before an interaction with the reflected shock could occur. To view the reflected shock interaction, the second test section was removed and the end plate placed on the back of the first test section. The distance between the jet and the end wall was 11.75 inches which allowed the reflected shock interaction to occur within the view of the window.

Considerations for Quantitative Analysis.

Dependence of the Signal on Pressure and Temperature

The objective of the quantitative analysis is to find the molar concentration field of helium from the light intensity field in the pictures taken with the CCD camera. The intensity of light measured by a pixel on the camera is related to the concentration field through:

$$\text{Signal} \sim n\,(\alpha_{air}\chi_{air}+\alpha_{He}\chi_{He})$$

where n is the number density of molecules, χ is the mole fraction, and α is the scattering cross section of the molecules. Since α_{air} is 66 times larger than α_{He}, pure air scatters 66 times more light than pure helium. Since the number density is a function of pressure and temperature, the signal also depends on the pressure and temperature.

Computations by Yang (1991) show that the largest pressure variation throughout the structure after the formation of the vortex pair is about 1% for a Mach 1.1 shock, and about 5% for a Mach 2.0 shock, which indicates that the pressure variation is about 1% for the M = 1.066 and 1.142 cases, and between 1% and 5% for the M = 1.50 case. Since it was not possible to account for these differences, the quantitative analysis assumes the pressure is constant in each picture. Furthermore, because the specific heat ratio is different between helium and air, the temperature of the helium after the shock will be higher than the temperature of the air. For example, for an isentropic compression with the same pressure ratio as a Mach 1.1 shock, the number density in Helium will be 2.3% lower than the number density in air. A first order correction for this error was made by assuming $n \sim (p_2/p_1)^{1/\gamma}$, where p_2/p_1 is the pressure ratio calculated from the normal shock relations for a perfect gas, and where γ (the specific heat ratio) was evaluated

locally in the picture as a function of the mole fraction of helium.

Resolution Limits of the Camera and Laser

The molar concentrations measured by the pixels of the CCD camera represent average values of the concentration over a small volume of fluid and over a short time. The volume of fluid was contained in a parallelepiped; the cross section of the parallelepiped was the square area defined by the area viewed by an individual camera pixel (0.06mm by 0.06 mm in the test section), and the length was the thickness of the laser sheet (1.5 mm). If the flow was purely two-dimensional the thickness of the laser sheet would not be very important. A shadowgraph picture of the jet side view for M = 1.142 and p_1 = 1 atm is shown in Figure 4; the dashed line indicates the location of the laser sheet plane. The picture shows that the flow is laminar and very two-dimensional in the region of the laser sheet cut. The jet is inclined at a 5 degree angle relative to the normal of the laser sheet. This implies that averaging perpendicular to the plane of the laser sheet over the sheet thickness is equivalent to averaging over a distance of (1.5mm)tan(5^o) or about two pixels in the plane of the laser sheet.

The length of time over which the average was taken was defined by the laser pulse length which was about 700 nsec. During this time, fluid elements of air behind shocks which have Mach numbers of 1.07, 1.14, and 1.50, will move respectively 0.43 pixels, 0.90 pixels and 1.9 pixels.

Estimate of the Scales of Interest

In order for the volumetric average of helium concentrations in this laminar flow to accurately represent the molecular concentration, the length scales over which changes in concentrations occur must be larger than the lengths of the averaging. Diffusion acts to increase the concentration length scale while the straining imposed by the vorticity generated by the shock shortens the length scale. This process is similar to that which occurs in the diffusion layers of a small flame element in a straining flow where it is found for fast chemical kinetics, a constant strain rate, and $\varepsilon t >> 1$ that the diffusion layer thickness for the fuel and oxidant are each about $(2\mathcal{D}/\varepsilon)^{1/2}$. Here $\mathcal{D}$ is the binary diffusion coefficient, and ε is the strain rate.

Because the strain rates are caused by the vorticity generated during the shock interaction it is reasonable to expect the strain rates in the flow to scale with Γ/d^2 and for the concentration length scales to scale with $\mathcal{D}/\Gamma$. For gases, the Schmidt number, $\nu/\mathcal{D}$ is about one and $\mathcal{D}/\Gamma \sim \nu/\Gamma$. The value of ν/Γ was smallest for the case where M = 1.14 and p_1 = 1 atm, and it is expected that this case will have the smallest concentration length scales of all the cases studied. For this case, in two pictures with times close together strain rates were estimated by measuring the length of an element of fluid in the strand of fluid which joins the top vortex and bottom vortex, and the length of an element of fluid in the core regions. The values $(1/L)(\Delta L/\Delta T)$ were calculated for both elements to be about 5000 sec^{-1}. These rates should be the highest strain rates in the flow and imply that the smallest diffusion scales should be about $2(2\mathcal{D}/\varepsilon)^{1/2}$ = 7 pixels. Since the averaging is over about 2 pixels, the measurements should accurately represent the helium concentrations.

Noise Considerations

The ratio of (scattering signal):(rms of signal) was found to be 30:1 for each pixel for pure air at atmospheric pressure. The noise in the signal is mostly due to shot noise, which results from the finite number of photons striking a pixel. The initial pressure before the shock wave had to be lowered for the higher Mach number experiments to keep the test section pressure behind the reflected shock within the safe limits of the structure. Since the number density of molecules was lower, the scattering signal was also reduced, and the ratio for pure air of the (signal):(rms signal) decreased. As mentioned earlier, this decrease caused the pictures for the higher Mach number cases to be more grainy than the pictures for the lower Mach number cases. Table 3 shows the ratio for the different cases.

Table 3

Case	(Air Signal)/(Rms of Signal)
M = 1.07, 1.14 p1 = 1 atm	30
M = 1.14 p1 = 0.55 atm	20
M = 1.50 p1 = 0.23 atm	15

Contour Plots

Contour plots of helium mole fractions were generated from the planar Rayleigh scattering images. In all the plots, the shock wave had moved from left to right, and hence the flow in the laboratory reference frame was from left to right. The vertical axis is defined as the 'y' axis, and y = 0 is the symmetry line of the structure which corresponds to the 'x' axis.

Mach 1.07 Shock Wave

Figure 5 is a sequence of contour plots of helium mole fractions for a cross section of a jet of helium (5.7 diameters above the jet exit) after the passage of a Mach 1.07 shock wave. The last plot in the sequence is for $a_1 t/r_0$ = 250 which is 2 or three times longer than the fuel residence time ($a_1 t/r_0$ = 80 to 160) estimated earlier.

Figure 5a shows the jet cross section after the diaphragm of the shock tube broke but 0.2 ms before the shock wave reaches the jet. As explained in previous investigations (Jacobs 1992, Yang 1991, Picone and Boris 1987), while the incident shock wave passes over the helium jet from left to right, vorticity is generated where the density gradients of the jet are not parallel to the pressure gradients of the shock wave. Counter clockwise vorticity is produced on the top of the cross section and clockwise vorticity on the bottom. As shown in Figure 5a through c, this vorticity first causes a stream of air to move through the center of the initially circular helium distribution, dividing the inhomogeneity into an upper lobe and a lower lobe connected by a thin strand of fluid. Each half is further divided into a back lobe or tail region, and a front lobe where computations (Picone and Boris 1988, Yang 1991) show most of the vorticity is concentrated. In Figure 5d the front lobes form a vortex pair which starts to pull ahead of the tail regions. As time progresses in Figure 5e through 5h, the vortex pair pulls further ahead of the tails, the tails are strained and grow thinner and longer.

In Figure 5c the highest concentrations of helium are in the tail and core region. As the sequence progresses in Figure 5 d, e, f, g, and h, the highest concentrations of helium in the tail regions decreases faster than the highest concentrations in the center of the vortex cores which shows that more mixing occurs in the tails than in the cores as the vortex pair moves ahead of and strains the tail regions.

Figures 5i through 5l show what happens when the reflected shock wave passes over the vortex pair at time a_1t/r_0 = 110 (just after 5d). Once again vorticity is baroclinically generated where the pressure and density gradients are not parallel. Counter-clockwise vorticity is generated on the top of each vortex and clockwise vorticiy is generated on the bottom of each vortex. In Figure 5i the structure has two tail regions; the first from the left is the original tail region before the reflected shock, and the second from the left is fluid which was originally in the core regions but has been stripped away by the vorticity generated by the reflected shock. As the original vortex cores split, the interfacial area between the air and helium increases and the mixing is further enhanced.

The reflected shock interaction also generates vorticity in the tail regions of Figure 5d. Before the reflected shock, the tails contained little vorticity, and the vorticity generated by the reflected shock interaction forms vortex pairs that are seen in Figure 5k. The clockwise vorticity that was generated on the outside edges of the original upper vortex core in Figure 5d, becomes a visible clockwise vortex in Figure 5l. Additional details of the effect of the reflected shock interaction are given in Budzinski (1992) and Yang (1991).

Higher Mach Numbers

A contour plot for a Mach 1.14 shock interaction after a time a_1t/r_0 = 46.2 is shown in Figure 6, and a plot for a Mach 1.50 shock interaction after a_1t/r_0 = 15.5 is shown in Figure 7 These two plots are at about the same stage in development as Figure 5d for the Mach 1.07 interaction. In general, the development of the vortex pair in the higher Mach number cases is very similar to the development in the Mach 1.07 case. The major difference as the shock Mach number increases is that the amount of helium in the tail regions decreases.

Mixing Measurements

Definition of the Mass Distribution Function

The objective of the study is to measure the molecular mixing between helium and air. In order to facilitate this a mass distribution function for each picture is defined which shows how the helium is distributed in different molar concentrations of helium for that picture. The mass distribution function, $m_{He}(\chi_{He})$ is defined such that:

$$m_{He}(\chi^0_{He})d\chi_{He} = \frac{(\#\text{ of moles in mole fraction range}\chi^0_{He}\text{ to }\chi^0_{He}+d\chi_{He})}{(\text{total \# of moles of helium})},$$

where χ_{He} is the mole fraction of helium and χ^0_{He} is a particular value of the mole fraction of helium. Formally the definition is:

$$m_{He}(\chi_{He}) = \frac{1}{M_{tot}}\frac{dM_{tot}}{d\chi_{He}},$$

where M_{tot} is the total number of moles of helium in the cross section. The mass distribution function has the property that:

$$1 = \int_0^1 m_{He}(\chi_{He})d\chi_{He} .$$

If the initial jet was a top hat profile of pure helium, the mass distribution function would be a delta function at χ_{He} = 1. On the other hand, if an initial finite mass of helium were allowed to mix uniformly with a very large amount of air, the distribution would approach a delta function at $\chi_{He} = 0^+$. For combustion between hydrogen and air the goal is to have as much mass as possible near the stoichiometric ratio of χ_{H_2} = 0.3.

For an individual picture, a box is drawn around the region which contains the helium. The mole fraction range from 0 to 1 is divided up into a finite number of bins. The number of bins used was set roughly equal to the dynamic range of the picture as defined by the ratio of

(signal of pure air)/(rms of the signal). For each pixel in the box the mole fraction of helium, and mass of helium were calculated. The mass of helium was added to the bin appropriate for the measured mole fraction. This results in the relation:

$$m_{He} \propto A(\chi^0_{He})\, n\, \chi^0_{He} \qquad \text{where}$$

$$A(\chi^0_{He}) \equiv \text{area of fluid with concentrations in the range } \chi^0_{He} \text{ to } \chi^0_{He} + d\chi_{He},$$

and n is the number density of molecules. This shows that the mass distribution function has an area weighting and concentration weighting. Nominally, the distribution would not be affected by the size of the box used in the calculation, as long as the box contained all of the helium mass. However, because there is noise in the signal, the distribution in the lowest mole fraction ranges will be affected by the size of the box. In addition, the pictures in general did not view all of the helium mass, but missed some of the mass in the lowest concentrations of helium.

The cross sections of the jets investigated did not have pure helium in the center of the jet. Air diffused into the center and premixed with the helium. To take this into account, the mole fractions of helium are converted to mole fractions of jet fluid χ_{jet}, by dividing the mole fractions of helium by the maximum helium mole fraction in the initial jet. Thus, $\chi_{jet} = 1$ represents the initial jet centerline mixture of air and helium at the cross section studied.

The general characteristics for the mass distribution for the initial helium jets are illustrated in Figure 8 in which two mass distributions for two different cross sections (one at 4.9 jet exit diameters above the jet exit, the other at 5.7) are shown. In general, the mass distribution function has the value 0, at $\chi_{jet} = 0$, because of the mole fraction weighting. Although on average pure air will be represented by $\chi_{jet} = 0$, the noise in the signal causes some pixels in regions with pure air to be brighter than average and some darker than average. The pure air pixels which are brighter than average result in negative concentrations and masses of jet fluid. The darker than average pure air signals add to the positive but low concentrations of jet fluid. In addition, noise in the signal near $\chi_{jet} = 1$ allows mole fraction values larger than 1. In the mole fraction range from 0 to 0.2, the distribution rises sharply. Part of this increase is produced by the noise, but a larger part represents the large mass of helium which is contained in this range. In the mole fraction range from 0.2 to 0.4 the distribution decreases. This change indicates that the area weighting is decreasing faster that the mole fraction weighting. The distribution is roughly level for mole fractions between 0.4 and 0.9, and this indicates a balance between the decrease in area and increase in mole fraction.

Because the average exit velocity of the jet was 130 cm/sec, an element of fluid takes 5 milliseconds (or $a_1 t/r_0 = 350$) to travel between the two cross sections. The small difference between the two curves in Figure 8 shows that little mixing occurs in the jet cross section over the 5 milliseconds.

In addition to drawing a box around the entire region containing the helium, boxes were drawn around the tail regions, and the vortex core regions as in Figure 9. This allows the contribution to the mixing in the core and tail regions to be studied separately in a qualitative sense since the representation of the distribution in the tails and cores depends on the size of the boxes drawn.

Mass Distributions for Mach numbers 1.066, 1.142, and 1.50.

The mass distribution function for the whole picture, the tail regions, and the core regions is shown in Figure 10 for M = 1.066 and $a_1 t/r_0 = 156$. There is no pure jet fluid left at this time. On the right side of the Figure, the mass distribution function increases (with decreasing mole fraction of jet fluid) from zero. The first rise with decreasing mole fraction represents the maximum concentrations of jet fluid left in the cross section. The curves for the whole picture and core regions are identical at the highest mole fractions. This indicates that the cores contain the regions with the highest helium concentrations. As the mole fraction continues to decrease, the curves separate as mass appears in the tail regions. The tails are shown to add a second distinct rise to the curve for the whole picture, and help to form a broad peak in the curve between mole fractions of 0.75 and 0.4. The second rapid rise represents the maximum jet fluid concentrations in the tails.

Figure 11 shows the total mass distribution curves for the initial jet and at three times after the shock interaction. When comparing the initial jet distribution with the first time shown of $a_1 t/r_0 = 85$, it is seen that the major effect of the shock is to move mass from the highest concentrations into a broad peak in the curve for $a_1 t/r_0 = 85$ which occurs in the concentration range 0.65 to 0.85. The distribution at $a_1 t/r_0 = 85$ below a mole fraction value of 0.5 is not much different than the initial jet distribution. Most of the mass that was above a mole fraction of 0.5 is still above 0.5.

For each of the times shown, the first slope from the right which brings the mass distribution function up from zero represents the maximum concentrations of jet fluid found in the vortex cores and in the entire picture. As time increases, this curve shifts to the left as more air is mixed in the center of the cores. For each time, there is a second slope from the right which represents the maximum jet fluid concentrations in the tails. The fact that the second slope from the right, shifts to the left faster than the first slope is an indication that the tails are being strained and mixed faster than the cores. The

difference in the mass distribution function for the initial jet and $a_1 t/r_0 = 204$, which corresponds to about 2.0 milliseconds, can be compared to the difference between the two curves in Figure 8. Much more mixing occurred in the cross section of the laser sheet after the shock interaction over two milliseconds, than occurred as a cross section of the jet moved from h/d = 4.9 to 5.7 over 5 milliseconds without a shock interaction.

Figure 12 shows the total mass distribution function and the contributions from the tails and vortex cores for M = 1.142 and p_1 = 0.55 atm. Previously it was noted that the tail regions were smaller in the M = 1.142 case than in the M = 1.066 case. Figure 12 also indicates that the contribution of the tails is much smaller here. The second slope from the right which represents the tails is much less pronounced. Figure 13 shows the total mass distribution for three different times. In this case the broad peak which forms is much less prominent than in the 1.066 case. At $a_1 t/r_0 = 28$, a more uniform shift of high concentrations to lower concentrations seems to have occurred than in the 1.066 case. Mass which was in concentrations above 0.5 has shifted below mole fractions of 0.55.

Figure 14 shows the mass distribution for the Mach 1.5 shock wave. The mass distribution in the tails is negligible here. Substantial mixing appears to have occurred even at the first time shown of $a_1 t/r_0 = 6$.

Mass of Jet Fluid in Regions at Least 30% and 50% Jet Fluid.

Another measure of the mixing is the mass of jet fluid contained in regions where the mole fraction of jet fluid is greater than 30% ($M_{30\%}$) or greater than 50% ($M_{50\%}$). These values are defined by the integrals:

$$M_{30\%} = \int_{0.3}^{1.0} m_{jet}(\chi_{jet})\, d\chi_{jet}, \text{ or } M_{50\%} = \int_{0.5}^{1.0} m_{jet}(\chi_{jet})\, d\chi_{jet}.$$

One value each of $M_{30\%}$ and $M_{50\%}$ is found for each experiment performed and curves of $M_{30\%}$ and $M_{50\%}$ are generated for each series of experiments. Figure 15 shows $M_{50\%}$ for Mach numbers 1.066, 1.142, and 1.50 vs. $a_1 t/r_0$. In order to emphasize the effect of the shock, the curves have been normalized by the initial values of $M_{50\%}$ in the jet cross sections before the shock interaction. Figure 15 shows that the mixing occurs much faster for the higher Mach numbers. Given the fact that the fuel may be in the engine for maximum times in the range $80 < a_1 t/r_0 < 160$, the mixing is found to be rapid enough to be of interest for supersonic combustion for shock Mach numbers in the range 1.15 to 1.50.

For the shock Mach number 1.07 case, the mass distribution functions showed (see Figure 10) that for early times the effect of the shock was to move the highest concentrations in the initial jet cross section, into a broad peak. Since the broad peak was located above the 0.5 mole fraction level, there is initially little change in $M_{50\%}$. As the broad peak shifts to lower concentrations the curve for $M_{50\%}$ decrease, reflecting the mixing which occurs.

Figure 16 plots $M_{50\%}$ vs. (t/τ) where τ is the characteristic time previously defined. This time scale provides a rough collapse of the mixing data. The time $(t/\tau) = 5$, is roughly the time it takes for the stream of air to move all the way through the initially circular jet cross section. As mentioned above $M_{50\%}$ does not change much initially for the M = 1.066 case, and it decreases only after $(t/\tau) = 5$. For the Mach 1.14 cases and the Mach 1.50 case, $M_{50\%}$ decreases almost immediately as the stream of air moves through the cross section before $(t/\tau) = 5$. This initial decrease is larger for the M = 1.50 case than for the M = 1.14 case. This indicates that as the shock Mach number increases, more mixing occurs initially as the stream of air moves through the cross section.

At later times, however, there is more mixing in the M = 1.066 case as the tails are strained by the vortex pair. The large tails for the lower Mach number allow $M_{50\%}$ for the M = 1.066 case to decrease below the values for the M = 1.14 cases, to about the same level as the M = 1.50 case. Figure 17 shows $M_{30\%}$ for the three Mach numbers. Overall, the behavior is similar to $M_{50\%}$.

Total Mass of Helium in the Cross section.

The total mass of helium for each picture (normalized by the initial total mass) can be used to check whether straining motions affect the cross section of the laser sheet and is shown in Figure 18 for shock Mach numbers of 1.07, 1.14, and 1.50. If the flow were purely two-dimensional, the total mass of helium in the cross section of the laser sheet would be constant as the time after the shock interaction increased. Small decreases in the total mass are observed for M = 1.07 and 1.14, while a small increase is observed for M = 1.50. These trends can be explained by the fact that the field of view of the camera was usually not large enough to see all of the helium present in the plane of the laser sheet. This is illustrated by defining the function:

$$m_x\left(\frac{x}{r_0}\right) = \int_{\left(\frac{y_1}{r_0}\right)}^{\left(\frac{y_2}{r_0}\right)} \frac{n}{n_{pure\ air}}\, \chi_{He}\, d\left(\frac{y}{r_0}\right),$$

which represents the distribution of helium mass along the x axis. Here n is the number density of molecules at a particular place in the picture, $n_{pure\ air}$ is the number

density of molecules in regions of pure air, χ_{He} is the molar concentration of helium, r_0 is the initial jet radius, y_1 is the y position at the bottom of the picture, and y_2 is the y position at the top of the picture. For example, in Figure 18 one of the largest decreases in the total mass of helium is for M = 1.066 with $a_1t/r_0 = 203$. For this case the total mass of helium is only 86% of the initial mass in the plane of the laser sheet and 14% of the mass is 'missing'. The distribution of helium mass along the x axis is shown in Figure 19 for M = 1.07 and $a_1t/r_0 = 203$. The distribution is not zero at the left edge of the figure, which indicates that additional mass is contained in the cross section of the laser sheet to the left of the camera's field of view. The vortex pair appears to leave behind a 'wake' which is not entirely viewed by the camera and contains some helium mass.

It should be noted that the measurement of the total mass of helium in the plane of the laser sheet is complicated by the fact that a significant amount of the helium mass is contained in regions of low helium concentration which are sensitive to small errors. The scattering technique employed measures air concentrations, and the helium concentrations are found by subtracting the air concentration from 1. In a region of 90% air, a 1% error in the molar air concentration would generate a 10% error in the mass of helium in that region.

The trend of increasing total mass for shock Mach number 1.50 in Figure 18 may also (at least partly) be explained by mass which initially is not within the view of the camera. In the contour plot for the Mach 1.5 case (figure 7) it is observed that the tail regions slightly extend above and below the camera's field of view. The tails receive an induced motion from the vortex pairs which tend to bring more of the tails within the view of the camera. As the time after the shock interaction increases, the mass of helium within the view of the camera increases.

Typically, the only regions affected by the fact that the camera did not view all of the helium in the plane of the laser sheet were regions where the molar helium concentration was less than 5%. The plots in Figures 15, 16, and 17 of $M_{50\%}/(M_{50\%})_{initial}$ and $M_{30\%}/(M_{30\%})_{initial}$ were not affected because all of the mass of helium in regions greater than 30% helium were within the view of the camera.

Since the change in total mass within the view of the camera is small, and that the change can be explained by the fact that the camera does not view all of the mass in the cross section, the loss of helium from the cross section due to straining motions normal to the plane of the laser sheet is not considered to have a significant effect on the mixing measurements.

The Effect of the Reflected Shock.

Earlier it was described how the reflected shock generated vorticity which tore part of the vortex cores away causing additional straining and deformation. Figure 20 compares two mass distribution functions at similar times; one developed after a reflected shock interaction at $a_1t/r_0 = 110$, while the other developed without a reflected shock interaction. The additional mixing caused by the reflected shock is shown by the shift to the left in the mass distribution from the case with no reflected shock to the case with a reflected shock. The additional enhancement in mixing is also shown in Figure 21 which gives the mass in regions greater than 30% and 50% for the Mach 1.066 case with and without the reflected shock. The reflected shock also enhances the mixing for M = 1.142 as shown in Figure 22.

Summary of the Mixing Results

To summarize the amount of mixing which occurs after the initial and reflected shock interactions, values of $M_{50\%}$ for the initial jet in each case and for the last picture in each case are given in Table 4 along with values of $M_{50\%}/(M_{50\%})_{initial}$.

As shown in the first row of Table 4, there is little difference between $M_{50\%}$ at h/D = 4.9 and h/D =5.7, which indicates that without a shock interaction little mixing occurs over a time interval of $a_1t/r_0 = 350$. In contrast, substantial mixing occurs over shorter time intervals with one or two shock interactions as shown in the rest of Table 4. A comparison of the values of a_1t/r_0 in Table 4 with the estimate of the time available for mixing in a supersonic combustion engine of $a_1t/r_0 = 80$ to 160 indicates that the mixing which occurs after a shock interaction happens fast enough (especially for shock Mach numbers above 1.15) to be of interest to the designers of supersonic combustion engines.

Conclusions

Planar Rayleigh scattering was used to study the enhancement in molecular mixing after a shock passes through a laminar jet of helium. Molar concentration fields in two-dimensional cross sections were determined at increasing times after the shock interaction. The shock Mach number was varied, and the effect of a reflected shock was studied.

The mixing in the two-dimensional cross sections of the jet is found to be significantly enhanced after the interaction of a shock wave compared to the mixing which would occur if the cross sections continued to travel in the direction of the jet without a shock interaction. Furthermore, the increased mixing occurs fast enough for shock Mach numbers in the range 1.15 - 1.50 to be useful in supersonic combustors.

For Mach number 1.066, at early times the center of the jet is mixed the most as the stream of air moves through the center of the jet. Little change occurs in the mass distribution function in the helium mole fraction values below 0.5. Relatively large tail lobes form. As

the vortex pair pulls ahead of the tail regions, the tails are strained and mixed.

As the Mach number increases, better mixing occurs as the stream of air moves through the center of the jet. As the Mach number increases, changes increase in the mass distribution function in the helium mole fraction values below 0.5 increase. The tail regions contain progressively less helium as the Mach number increases. Less mixing occurs at the later times since less mass is strained in the tails as the vortex pair pulls ahead. A rough collapse of the mixing data occurs when time is normalized with the jet radius divided by the velocity of the air behind the shock, which is consistent with the development time of Yang (1991).

The vorticity generated by the reflected shock tears away and strains part of the vortex cores. The tail regions are also additionally strained by the reflected shock. An increase in the enhancement in the mixing occurs. The core regions remaining after the reflected shock are closer together.

Table 4

Case	$(a_1 t/r_0)_{final}$	$(M_{50\%})_{initial}$	$(M_{50\%})_{final}$	$M_{50\%}/(M_{50\%})_{initial}$
Initial Jet as Cross-Section Moves from h/D=4.9 to 5.7 (No Shocks)	350	0.47	0.45	0.96
M=1.066 Initial Shock Only	250	0.45	0.20	0.45
M=1.066 Initial and Reflected Shocks	202	0.45	0.12	0.27
M=1.146, P=1 atm Initial Shock Only	74	0.46	0.30	0.66
M=1.142, P=0.55 atm Initial Shock Only	107	0.45	0.27	0.59
M=1.142 , P=0.55 atm Initial and Reflected Shocks	120	0.45	0.17	0.38
M=1.50 Initial Shock Only	26	0.39	0.20	0.53

References

Bohren, B. F., Huffman, D. R. (1983), Absorption and Scattering of Light by Small Particles, John Wiley & Sons, New York.

Budzinski, J. M. (1992), "Planar Rayleigh Scattering Measurements of Shock Enhanced Mixing," Ph.D. Thesis, California Institute of Technology, Pasadena, Califronia.

Drummond, J. P., Carpenter, M. H., Reggins, D. W., and Adams, M. S. [1989], "Mixing Enhancement in a Supersonic Combustor," AIAA/ASME/SAE/ASEE 25th Joint Propulsion Conference, AIAA Paper 89-2794.

Eckbreth, A. C. (1988), Laser Diagnostics for Combustion Temperature and Species, Abacus Press, Tunbridge Wells, Kent.

Haas, F., and Sturtevant, B. [1987], "Interaction of Weak Shock Waves with Cylindrical and Spherical Gas Inhomogeneities," J. Fluid Mechanics, v. 181, pp. 41-76.

Jacobs, J. W. [1992], "Shock-Induced Mixing of a Light-Gas Cylinder," J. Fluid Mechanics, v. 234, pp. 629-649.

Liepmann, H. W., Roshko, A., Coles, D., and Sturtevant, B. [1962], "A 17-inch Diameter Shock Tube for Studies in Rarefied Gas Dynamics," Rev. Sci. Instrum. 33, pp. 625-631.

Marble, F. E., Hendricks, G. J., and Zukoski, E. E. [1987], "Progress Toward Shock Enhancement of Supersonic Combustion Processes," AIAA/SAE/ASME/ASEE 23rd Joint Propulsion Conference, AIAA Paper 87-1880.

Marble, F. E., Zukoski, E. E., Jacobs, J. W., Hendricks, G. J., and Waitz, I. A. [1990], "Shock Enhancement and Control of Hypersonic Mixing and Combustion," AIAA/SAE/ASME/ASEE 26th Joint Propulsion Conference, AIAA Paper 90-1981.

Papamoschou, D., and Roshko, A. [1988], "The Compressible Turbulent Shear Layer: An Experimental Study," J. Fluid Mechanics, v. 197, pp. 453-477.

Picone, J. M. and Boris, J. P. [1988], "Vorticity Generation by Shock Propagation Through Bubbles in a Gas," J. Fluid Mechanics, v. 189, pp. 23-51.

Rudinger, G. and Somers, L. M. (1960), "Behavior of Small Regions of Different Gases Carried in Accelerated Gas Flows," J. Fluid Mechanics, v. 7, pp. 161-176.

Waitz, I. A. [1991], "An Investigation of Contoured Wall Injectors for Hypervelocity Mixing Augmentation," Ph.D. Thesis, California Institute of Technology, Pasadena, California.

Waitz, I. A., Marble, F. E., and Zukoski, E.E. [1991], "An Investigation of a Contoured Wall Injector for Hypervelocity Mixing Augmentation," AIAA/SAE/ASME/ASEE 27th Joint Propulsion Conference, AIAA Paper 91-2265.

Waitz, I. A., Marble, F. E., and Zukoski, E.E. [1992], "A Systematic Experimental and Computational Investigation of a Class of Contoured Wall Fuel Injectors," 30th Aerospace Sciences Meeting & Exhibit, AIAA Paper 92-0625.

Yang, J. [1991], "An Analytical and Computational Investigation of Shock-Induced Vortical Flows with Applications to Supersonic Combustion," Ph.D. Thesis, California Institute of Technology, Pasadena, California.

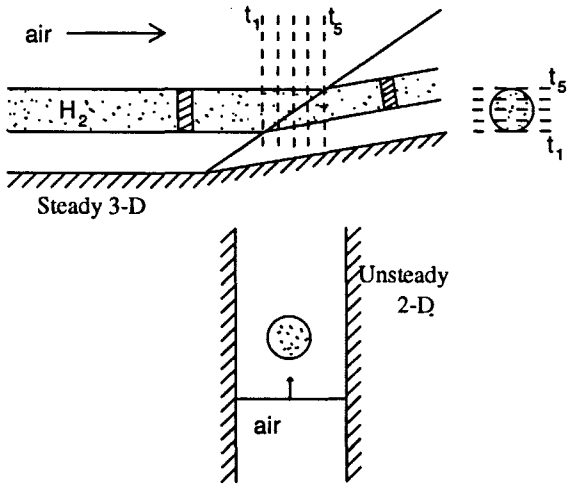

Figure 1. Comparison of 3-D steady and 2-D unsteady flows.

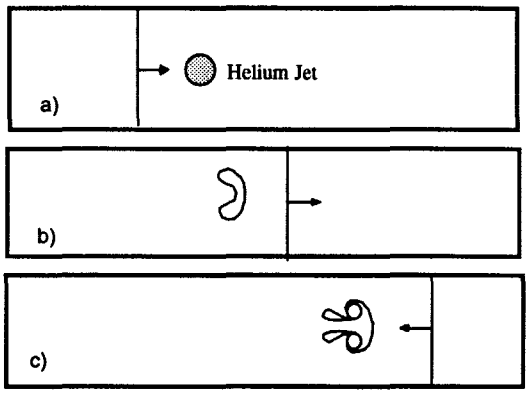

Figure 2. Description of the Experiment. a) Helium Jet Flows Out of the Page, Shock Travels Left to Right. b) Helium Jet Deformes. c) Vortex Pair Formes, Shock Reflects Off the End Wall and Travels Back Right to Left.

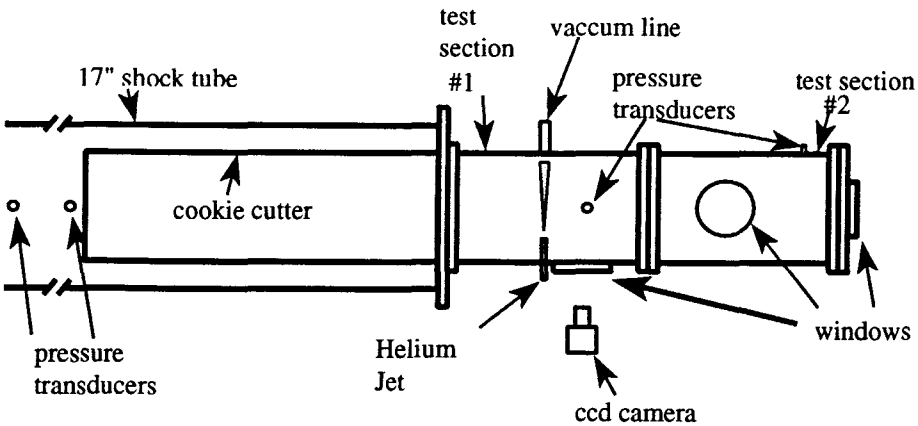

Figure 3. Side view of the 17 Inch Shock Tube Facility.

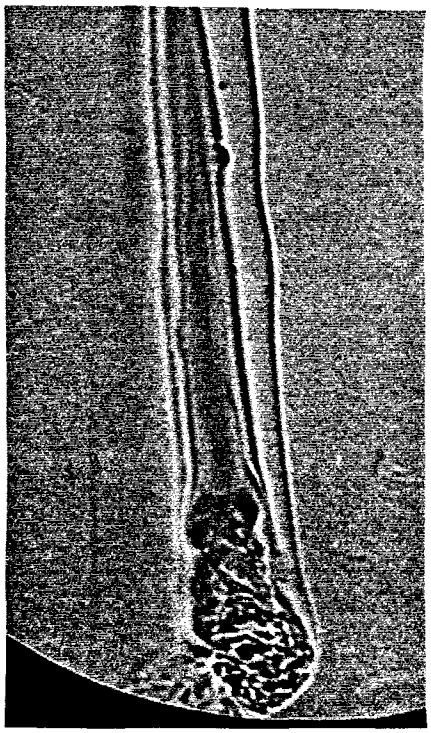

Figure 4. Shadowgraph of a Mach 1.14 Shock Interaction

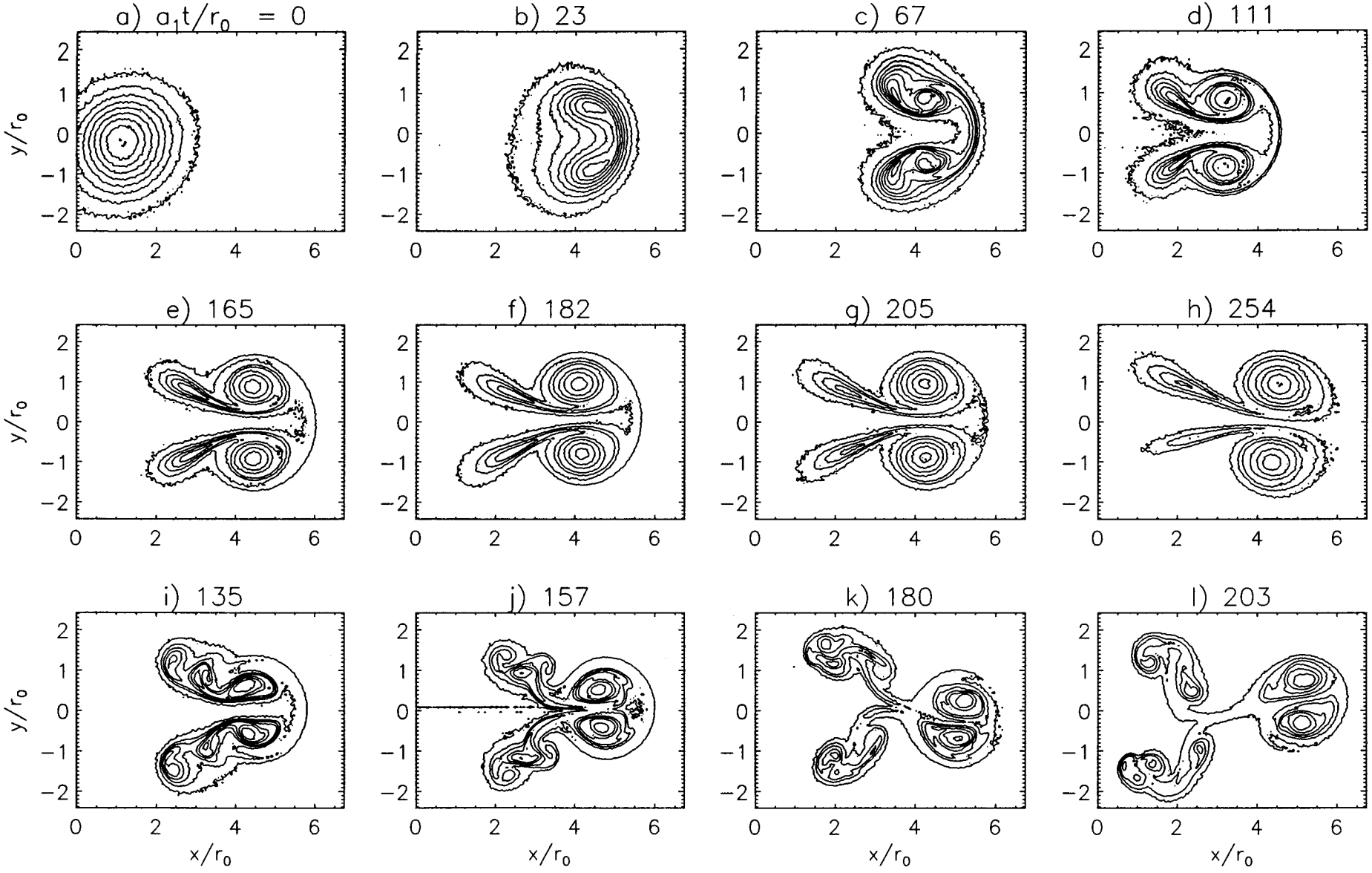

Figure 5. Contour Plots of Helium Mole Fractions (levels at 0.10 intervals) After a Mach 1.066 Shock Wave. Figures a) Through h) Were After the Initial Wave Only. Figures i) Through l) Were After the Initial Wave and a Reflected Shock at a_1t/r_0 = 110.

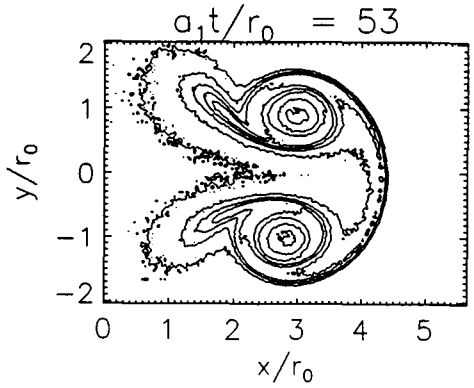

Figure 6. Contour Plot of Helium Mole Fractions After a Mach 1.14 Shock Wave.

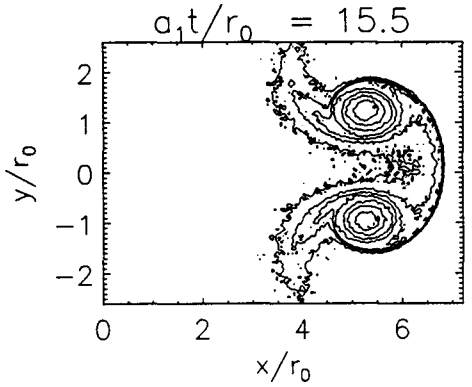

Figure 7. Contour Plot of Helium Mole Fractions After a Mach 1.50 Shock Wave.

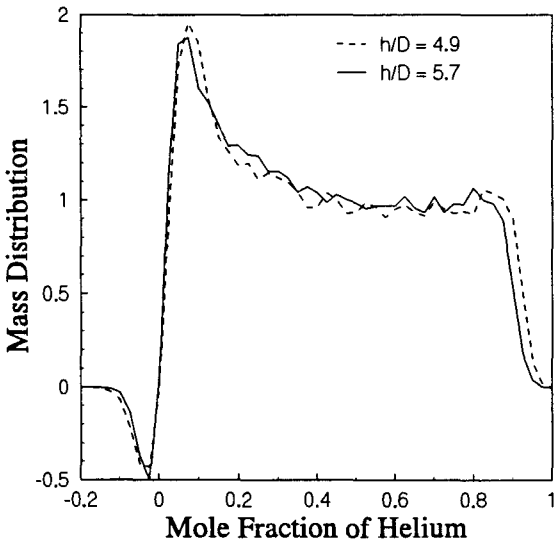

Figure 8. Mass Distribution Function for Two Initial Jet Cross Sections, One at h/D = 4.9, and the Other at h/D = 5.7

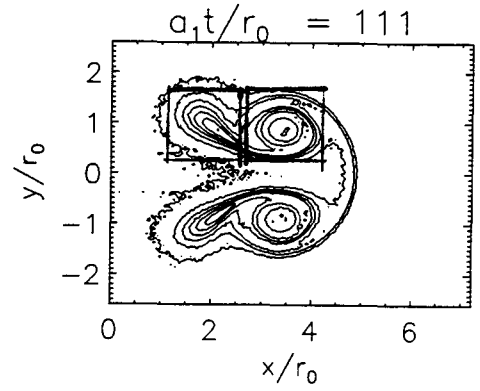

Figure 9. Example of Boxes Drawn Around the Tail and Core Regions.

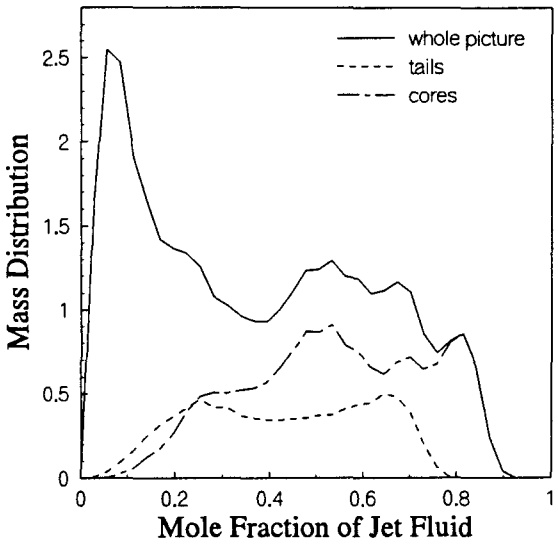

Figure 10. Mass Distribution Function for M = 1.066, a_1t/r_0 = 156.

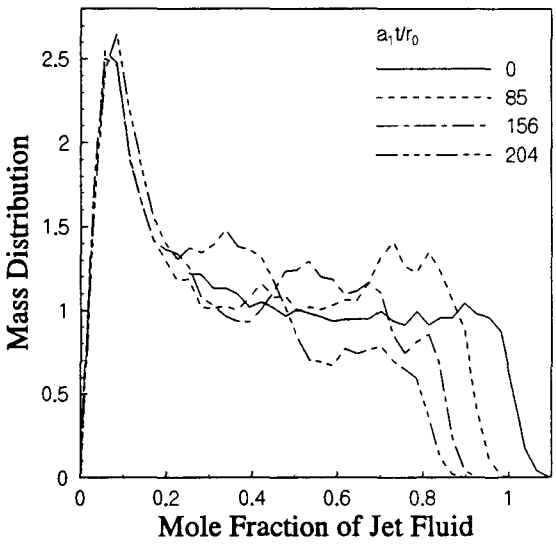

Figure 11. Mass Distribution Function for M = 1.066, a_1t/r_0 = 0, 85, 156, and 204.

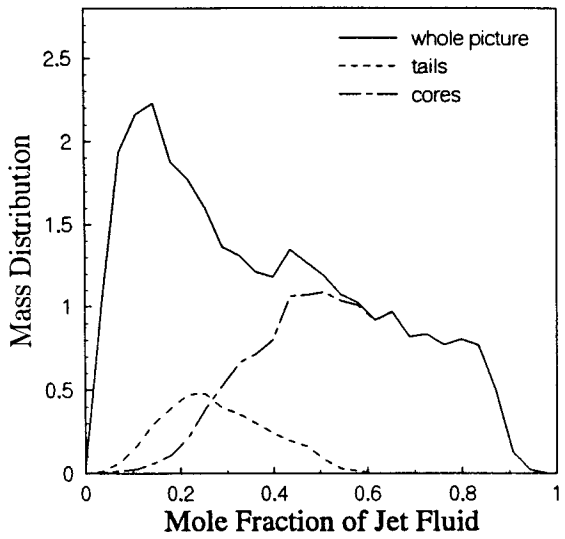

Figure 12. Mass Distribution Function for M = 1.142, $a_1t/r_0 = 64$.

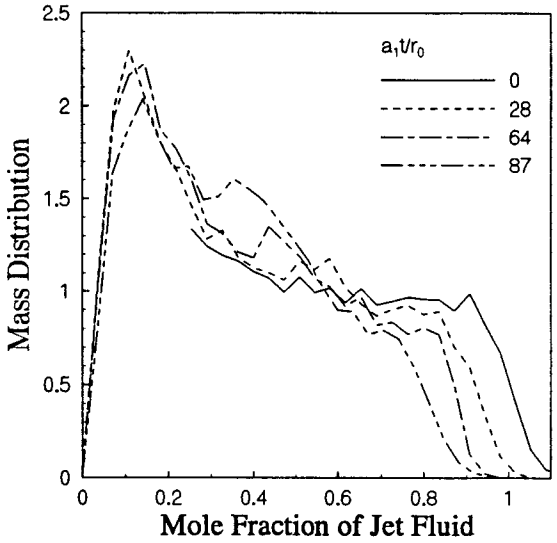

Figure 13. Mass Distribution Function for M = 1.142, $a_1t/r_0 = 0$, 28, 64, and 87.

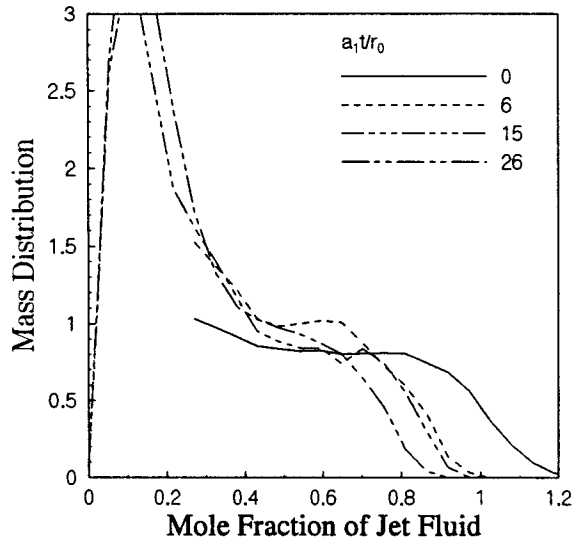

Figure 14. Mass Distribution Function for M = 1.50, $a_1t/r_0 = 0$, 6, 15, and 26.

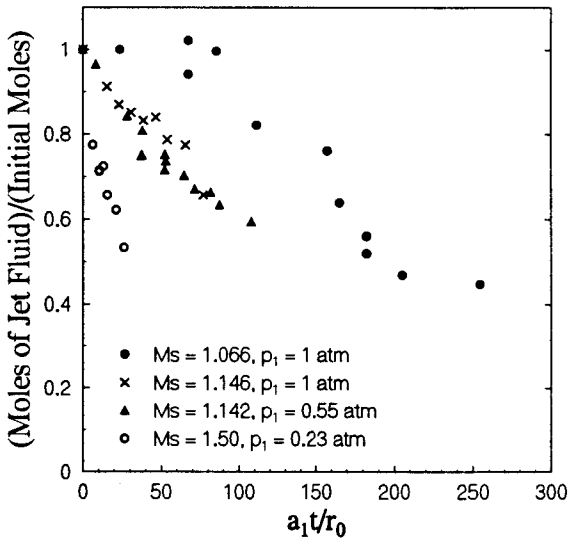

Figure 15. Mass of Jet Fluid in Regions Greater than 50% Jet Fluid vs. a_1t/r_0, M = 1.066, M = 1.142, M = 1.146, and M = 1.50.

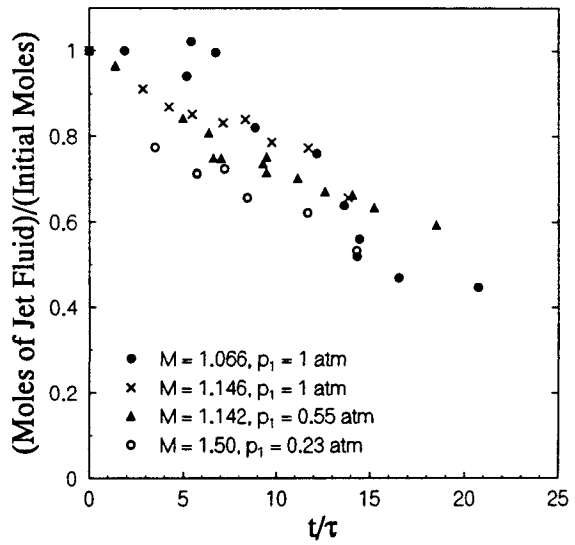

Figure 16. Mass of Jet Fluid in Regions Greater than 50% Jet Fluid. M = 1.066, M = 1.142, and M = 1.50.

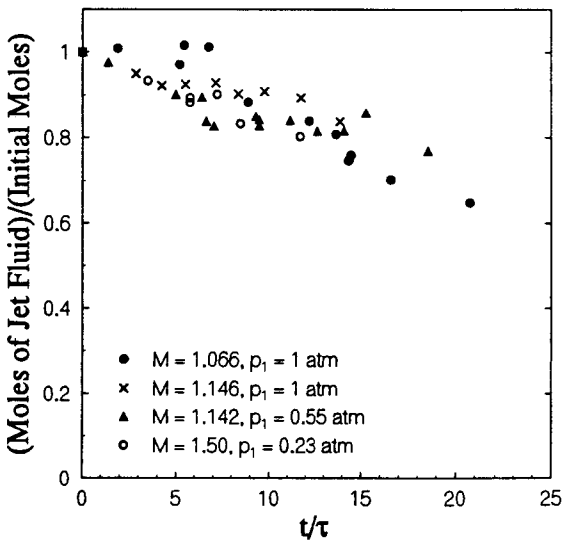

Figure 17. Mass of Jet Fluid in Regions Greater than 30% Jet Fluid. M = 1.066, M = 1.142, and M = 1.50.

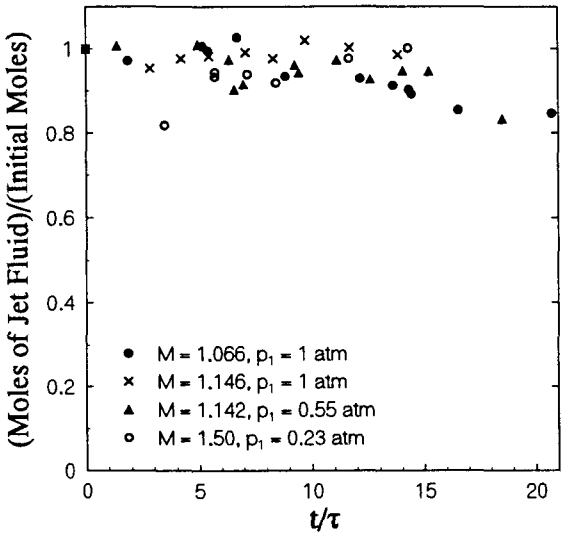

Figure 18. Total Mass of Jet Fluid.

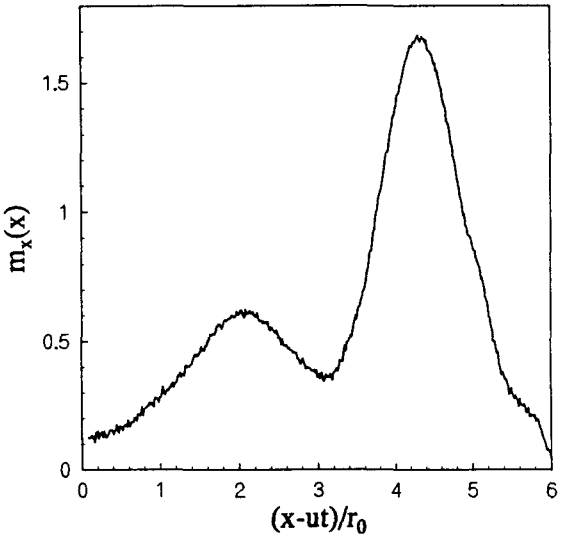

Figure 19. Distribution of Mass Along the X Axis $t/\tau = 16.5$, $M = 1.066$.

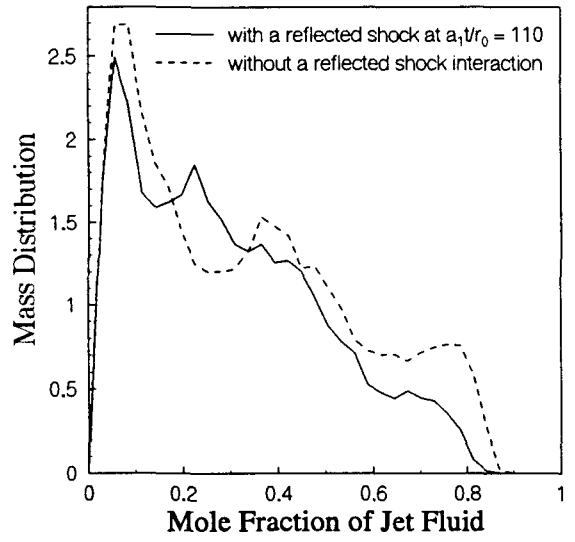

Figure 20. Mass Distribution Function for $M = 1.066$, $a_1 t/r_0 = 180$, Without a Reflected Shock Interaction, and With a Reflected Shock Interaction at $a_1 t/r_0 = 110$.

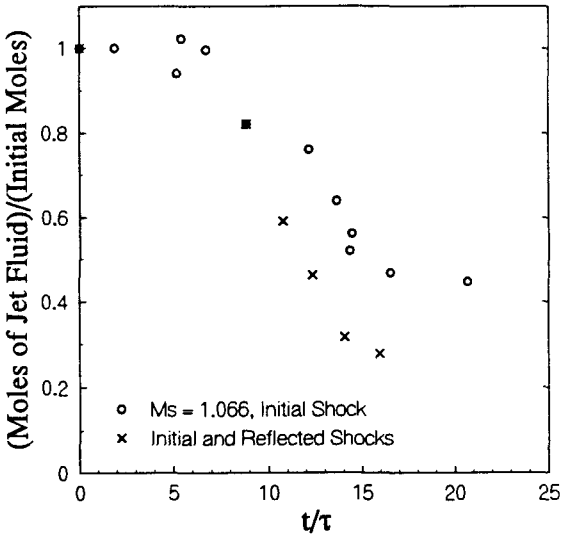

Figure 21. Mass of Jet Fluid in Regions Greater than 50% Jet Fluid, With and Without the Reflected Shock. $M = 1.066$.

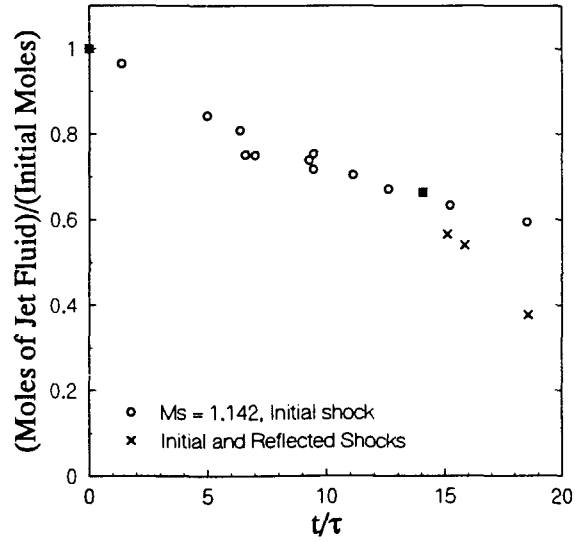

Figure 22. Mass of Jet Fluid in Regions Greater than 50% Jet Fluid, With and Without the Reflected Shock. $M = 1.142$.